Обзор ArXiv/astro-ph 19-24 сентября 2019

От Сильченко О.К.

ArXiv: 1909.09080

A BREAK IN SPIRAL GALAXY SCALING RELATIONS AT THE UPPER LIMIT OF GALAXY MASS

PATRICK M. OGLE[1], THOMAS JARRETT[2], LAURANNE LANZ[3], MICHELLE CLUVER[4,5], KATHERINE ALATALO[1], PHILIP N. APPLETON[6], JOSEPH M. MAZZARELLA[6]

[1]Space Telescope Science Institute, Baltimore, Maryland
[2]University of Cape Town, South Africa
[3]The College of New Jersey, Ewing, New Jersey
[4] Swinburne University of Technology, Melbourne, Australia
[5] Department of Physics and Astronomy, University of the Western Cape, South Africa and
[6] IPAC, California Institute of Technology, Pasadena, CA

Draft version September 20, 2019

ABSTRACT

Super spirals are the most massive star-forming disk galaxies in the universe (Ogle et al. 2016, 2019). We measured rotation curves for 23 massive spirals[a] and find a wide range of fast rotation speeds (240-570 km s^{-1}), indicating enclosed dynamical masses of $0.6 - 4 \times 10^{12} M_\odot$. Super spirals with mass in stars $\log M_{\rm stars}/M_\odot > 11.5$ break from the baryonic Tully-Fisher relation (BTFR) established for lower mass galaxies. The BTFR power-law index breaks from 3.75 ± 0.11 to 0.25 ± 0.41 above a rotation speed of ~ 340 km s^{-1}. Super spirals also have very high specific angular momenta that break from the Fall (1983) relation. These results indicate that super spirals are undermassive for their dark matter halos, limited to a mass in stars of $\log M_{\rm stars}/M_\odot < 11.8$. Most giant elliptical galaxies also obey this fundamental limit, which corresponds to a critical dark halo mass of $\log M_{\rm halo}/M_\odot \simeq 12.7$. Once a halo reaches this mass, its gas can no longer cool and collapse in a dynamical time. Super spirals survive today in halos as massive as $\log M_{\rm halo}/M_\odot \simeq 13.6$, continuing to form stars from the cold baryons they captured before their halos reached critical mass. The observed high-mass break in the BTFR is inconsistent with the Modified Newtonian Dynamics (MOND) theory (Bekenstein & Milgrom 1984).

Выборка и наблюдения

radii of up to ~ 50 kpc. We use optical long-slit spectroscopy of the Hα line to measure the rotation curves of 23 massive spirals and place them on the BTFR.

We assume a ΛCDM cosmology with $H_0 = 70$ km s^{-1} Mpc^{-1}, $\Lambda = 0.7$ and $\Omega = 0.3$ to derive all distances, linear sizes, and luminosities.

2. SAMPLE AND OBSERVATIONS

We selected our rotation curve sample (Table 1) from parent samples selected by r-band or K_s-band luminosity. First, we selected galaxies with inclination $i > 39°$ from the OGC sample of super spirals with $z < 0.3$ and Sloan Digital Sky Survey (SDSS) r-band luminosity $> 8L*$ (Ogle et al. 2019). Next, because extinction in the disk limits the number of high-inclination galaxies in the OGC, we created a new sample of IR-selected massive spirals drawn from the set of 2 Micron All-Sky Survey Extended Source Catalog (2MASX) galaxies with SDSS-measured redshifts, $i > 39°$, K_s-band luminosity $L(K_s) > 2\times10^{11} L_\odot(K_s)$, and r-band isophotal diameter $D_{25} > 50$ kpc. The K_s-band luminosity and D_{25} criteria were designed to yield a sample that overlaps Ogle et al. (2019) super spirals, which have $M_{\rm stars} > 2 \times 10^{11} M_\odot$ and $D_{25} > 55$ kpc.

We observed 3 massive spirals with the Double Spectrograph (DBSP) on the Hale Telescope and 20 with the

RSS/SALT

Пример САМОЙ массивной спиральной галактики (SALT)

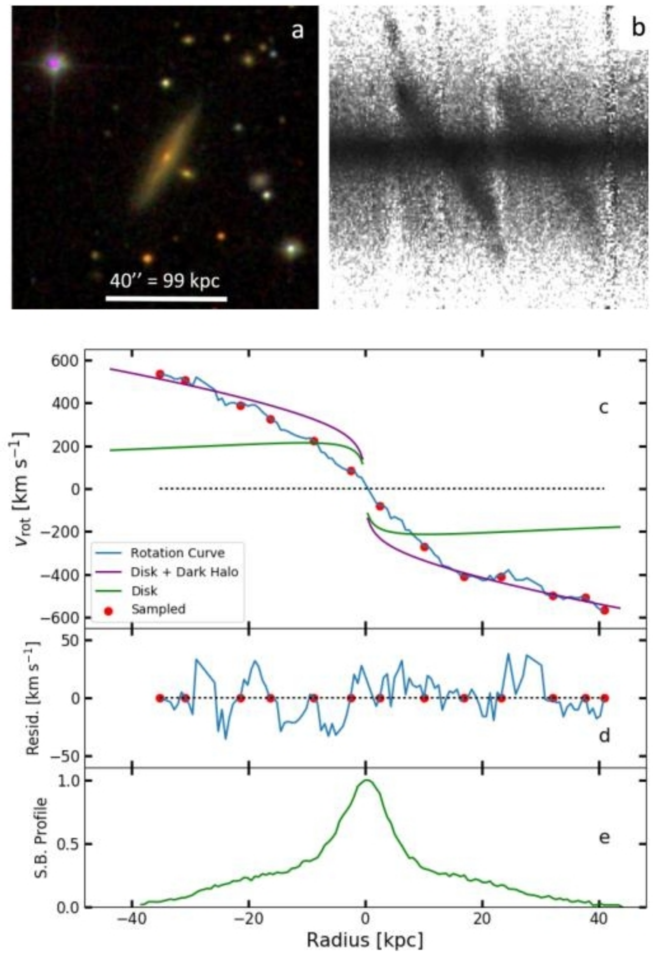

Disk+NFWгало

Самые массивные спирали отовсюду отклоняются

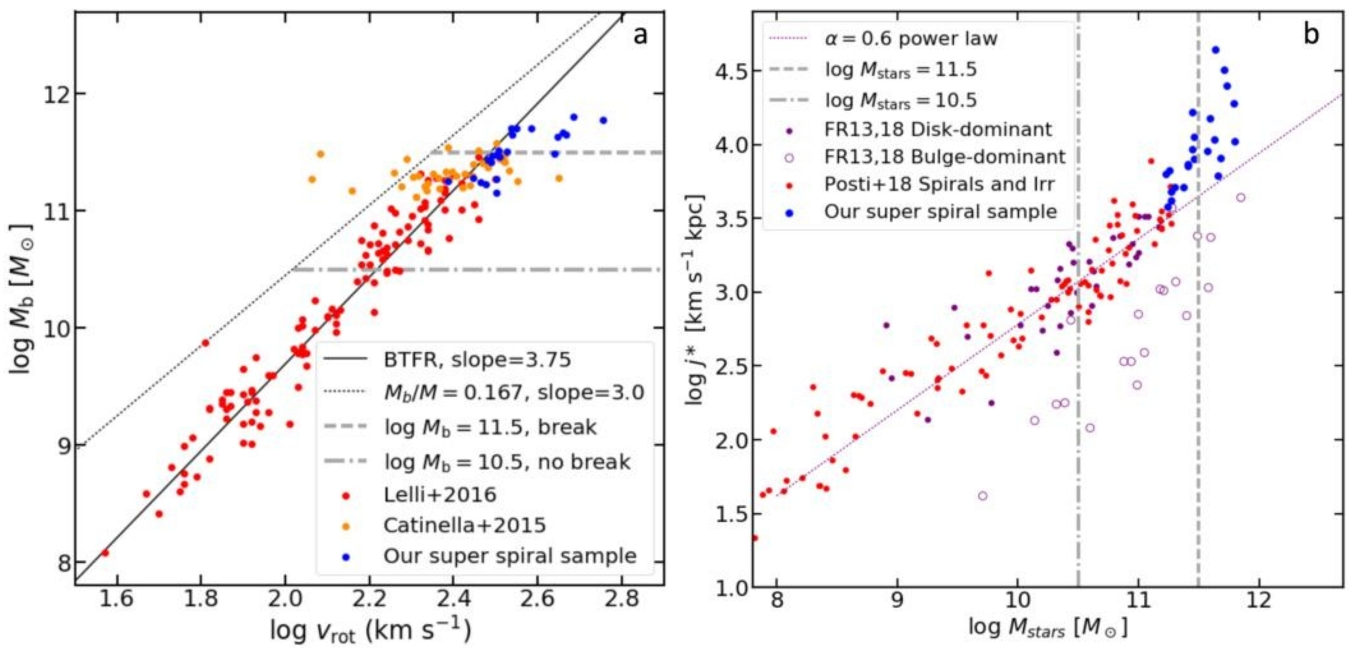

Figure 2. Baryonic Tully-Fisher relation (BTFR) and Fall (1983) relation. A break in both relations is found at a critical stellar mass of $\log M_{\rm stars}/M_\odot = 11.5$ (dashed lines). This is a factor of 10 greater than the characteristic mass of $\log M_{\rm stars}/M_\odot = 10.5$ at the break in the galaxy SMHM relation. a) BTFR. Masses in stars for the super spiral and comparison samples are estimated using custom *WISE* $W1$-band photometry, assuming $M/L = 0.6$. The photometric uncertainty is smaller than the size of the plot symbols (0.01-0.02 dex). Gas masses for the comparison samples are estimated as $M_{\rm gas} = 1.33 \times M_{\rm HI}$ (Lelli et al. 2016; Catinella & Cortese 2015), while gas masses for our sample are estimated using the Kennicutt (1998) Schmidt law, with uncertainties < 0.05 dex (see main text). The observed BTFR (data points) is compared to the Lelli et al. (2016) power-law fit (solid line) and the $v^3_{\rm rot}$ power-law for baryon fraction equal to the cosmic mean value (dotted line). b) Fall (1983) relation between galaxy specific angular momentum and mass in stars. The specific angular momenta of our sample galaxies are estimated by $j_* = 2R_d v_{max}$. We compare to disk-dominant spirals with bulge-to-disk mass ratios $\beta_* < 0.15$ and bulge-dominant ($\beta_* > 0.70$) ellipticals from Fall & Romanowsky (2013, 2018) and spirals and dwarf irregulars from Posti et al. (2018). Super spirals have exceedingly high specific angular momenta compared to lower mass spirals and deviate from the Fall relation (purple dotted line; Fall & Romanowsky 2018). The relation for elliptical galaxies is steeper and offset to lower j_*.

Есть предел звездной массы галактики?

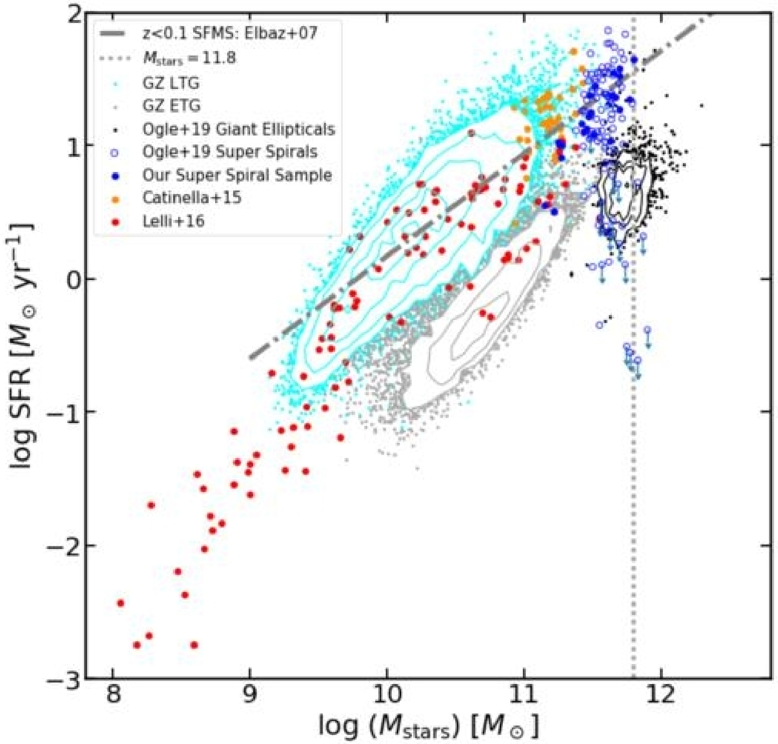

Figure 3. Star-forming main sequence (SFMS) (adapted from Ogle et al. 2019), with our rotation curve sample, BTFR comparison samples, and Galaxy Zoo (GZ) early type and late type galaxies over-plotted. The observed cosmic mass limit for spiral galaxies at $\log M_{\rm stars} = 11.8$ is indicated by the vertical dotted line. Super spirals fall along an extrapolation of the Elbaz et al. (2007) relation. Most giant ellipticals and lenticulars in the Ogle et al. (2019) sample respect the cosmic mass limit for spiral galaxies. The ones that do not may be the product of major mergers.

ArXiv: 1909.09306

Star-Forming, Rotating Spheroidal Galaxies in the GAMA and SAMI Surveys

Amanda J. Moffett,[1,2†] Steven Phillipps,[3] Aaron S. G. Robotham,[4] Simon P. Driver,[4] Malcolm N. Bremer,[3] Luca Cortese,[4,5] O. Ivy Wong,[4] Sarah Brough,[6] Michael J. I. Brown,[7] Julia J. Bryant,[5,8,9] Christopher J. Conselice,[10] Scott M. Croom,[5,6] Koshy George,[11,22] Greg Goldstein,[12] Michael Goodwin,[9] Benne W. Holwerda,[13] Andrew M. Hopkins,[15] Iraklis S. Konstantopoulos,[14] Jon S. Lawrence,[15] Nuria P. F. Lorente,[9] Anne M. Medling,[16,17,18] Matt S. Owers,[12] Kevin A. Pimbblet,[19] Samuel N. Richards,[20] Sarah M. Sweet,[5,21] and Jesse van de Sande[5,8]

[1] *Department of Physics and Astronomy, Vanderbilt University, PMB #401807 2401 Vanderbilt Place, Nashville TN 37240, USA*
[2] *Department of Physics and Astronomy, University of North Georgia, 3820 Mundy Mill Rd., Oakwood GA 30566, USA*
[3] *School of Physics, University of Bristol, Tyndall Avenue, Bristol BS8 1TL, UK*
[4] *ICRAR, The University of Western Australia, 35 Stirling Highway, Crawley WA 6009, Australia*
[5] *ARC Centre of Excellence for All Sky Astrophysics in 3 Dimensions (ASTRO 3D)*
[6] *School of Physics, University of New South Wales, NSW 2052, Australia*
[7] *School of Physics and Astronomy, Monash University, VIC 3800, Australia*
[8] *Sydney Institute for Astronomy, School of Physics, A28, The University of Sydney, NSW, 2006, Australia*
[9] *Australian Astronomical Optics, 105 Delhi Rd, North Ryde, NSW 2113, Australia*
[10] *School of Physics & Astronomy, University of Nottingham, Nottingham NG7 2RD, UK*
[11] *Indian Institute of Astrophysics, 2nd Block, Koramangala, Bangalore - 560034, India*
[12] *Department of Physics and Astronomy, Macquarie University, NSW 2109, Australia*
[13] *Department of Physics and Astronomy, 102 Natural Science Building, University of Louisville, Louisville KY 40292, USA*
[14] *Atlassian, 341 George St Sydney, NSW 2000, Australia*
[15] *Australian Astronomical Optics, Macquarie University, 105 Delhi Rd, North Ryde, NSW 2113, Australia*
[16] *Ritter Astrophysical Research Center University of Toledo Toledo, OH 43606, USA*
[17] *Research School for Astronomy & Astrophysics Australian National University Canberra, ACT 2611, Australia*
[18] *Hubble Fellow*

Выборка

- Из обзора GAMA: 180 квадратных градуса вблизи экватора
- Визуальная морфологическая классификация: форма и цвет
- r<19.8
- 0.002<z<0.06
- 868 LBS (‘Little Blue Spheroid’)
- Потом фотометрия из обзора KiDS (VST)
- Потом кинематика из обзора SAMI

Вот так они выглядят в цвете

(a) (b) (c)

Figure 1. Representative LBS galaxies (GAMA IDs G300372, G418795, and G417568) in their original three-colour (giH) classification images. Classification images are 30kpc on a side in size (Moffett et al. 2016a), and all images are scaled using the same algorithm (tanh scaling) such that scaling differences reflect the changing dynamic range in each image (for example, the scaling in the far right panel is affected by a nearby bright point source).

По массе и темпам SF похожи на спирали совсем поздних типов

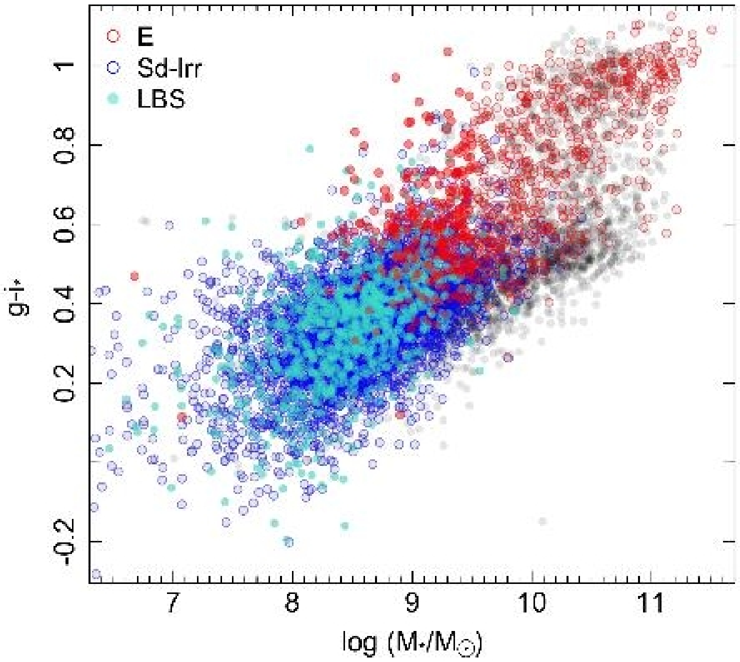

Figure 2. GAMA Visual Morphology sample in colour vs. stellar mass space, where $g-i_*$ is the intrinsic (corrected for internal dust extinction) $g-i$ colour from the SED modeling of Taylor et al. (2011). Stellar mass estimates are also derived from Taylor et al. (2011). Light grey points indicate the full sample distribution with coloured points indicating the E, Sd-Irr, and LBS classes. The subsample of "low-mass E" galaxies is indicated in filled red points.

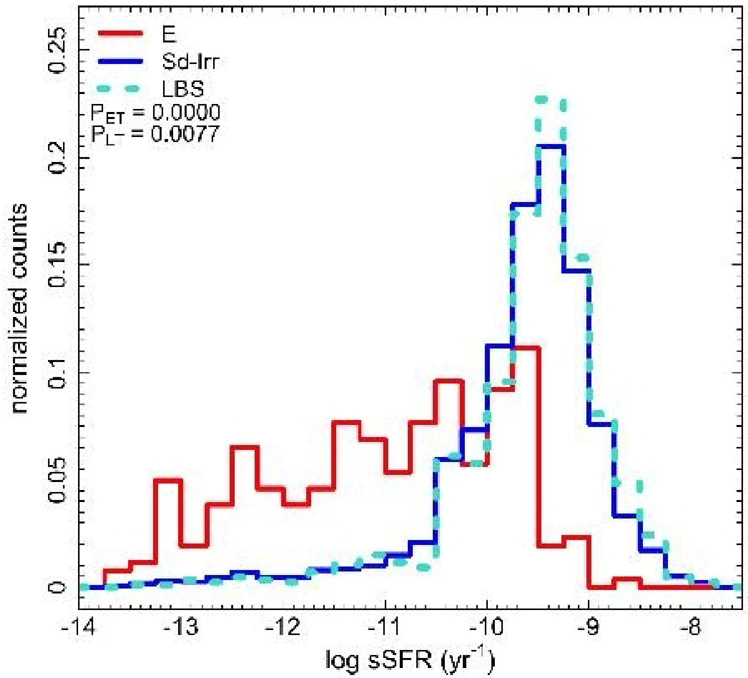

Figure 3. Distribution of LBS specific star formation rates compared to those of Sd-Irr and low-mass E galaxies, illustrating similar LBS and Sd-Irr star formation levels. The legend indicates p-values derived from K-S tests comparing the LBS property distribution to those of low-mass E (P_{ET}) and Sd-Irr (P_{LT}) populations.

ОЧЕНЬ разреженное окружение, практически изолированные

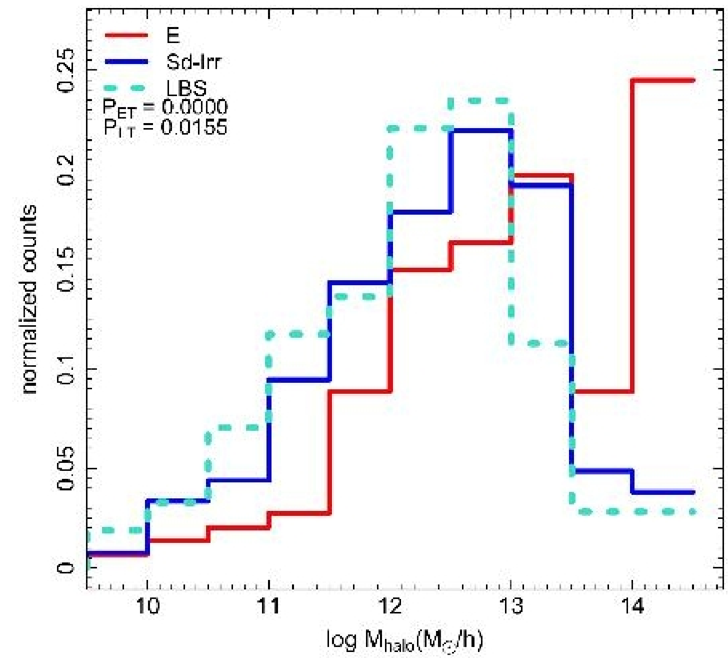

Figure 7. Distribution of LBS group halo masses compared to those of Sd-Irr and low-mass E galaxies, where LBSs tend to inhabit lower group halo mass environments than low-mass E galaxies and potentially slightly lower group halo mass environments than Sd-Irr galaxies as well. The legend indicates p-values derived from K-S tests comparing the LBS property distribution to those of low-mass E (P_{ET}) and Sd-Irr (P_{LT}) populations.

А вот по форме и размерам они похожи на эллиптические ТЕХ ЖЕ масс

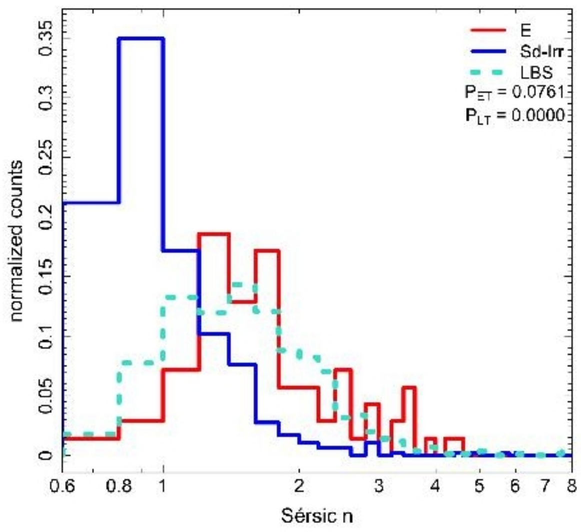

Figure 10. Distribution of LBS single Sérsic n values compared to Sd-Irr and low-mass E galaxies, illustrating that the LBS Sérsic n distribution is most similar to that of low-mass Es, albeit somewhat skewed to lower values. The legend indicates p-values derived from K-S tests comparing the LBS property distribution to those of low-mass E (P_{ET}) and Sd-Irr (P_{LT}) populations.

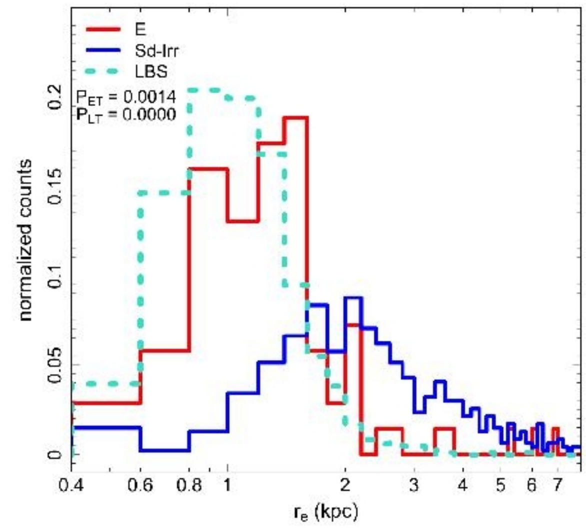

Figure 11. Distribution of LBS effective radius values (in kpc) compared to Sd-Irr and low-mass E galaxies, illustrating that the LBS effective radius distribution is similar to that of low-mass Es with a slight skew towards smaller size. The legend indicates p-values derived from K-S tests comparing the LBS property distribution to those of low-mass E (P_{ET}) and Sd-Irr (P_{LT}) populations.

И явно толстенькие

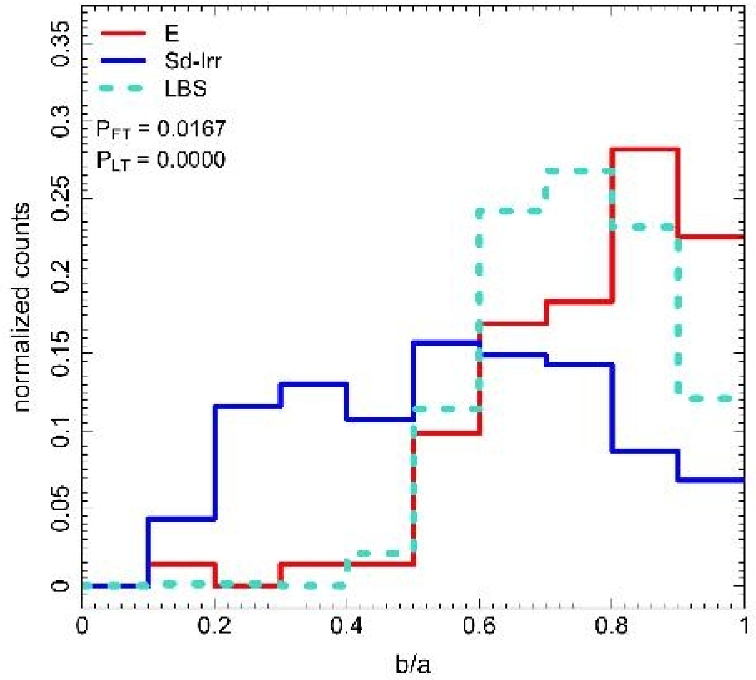

Figure 12. Distribution of LBS axial ratios compared to Sd-Irr and low-mass E galaxies, illustrating that the LBS axial ratio distribution is more similar to low-mass Es than Sd-Irrs. The legend indicates p-values derived from K-S tests comparing the LBS property distribution to those of low-mass E (P_{ET}) and Sd-Irr (P_{LT}) populations.

Панорамная спектроскопия в обзоре SAMI

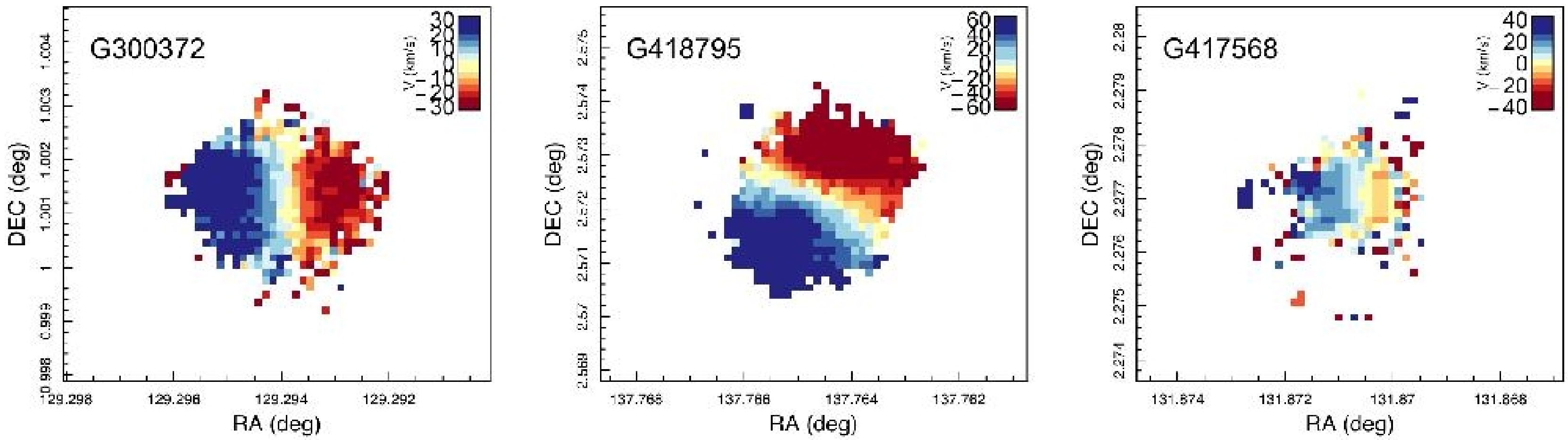

Figure 13. SAMI emission line velocity maps derived from the analysis described by Green et al. (2018) and Medling et al. (2018). The left and middle panels show examples of LBS galaxies with velocity fields that display extended, regular rotation well fit by the symmetric rising rotation curve form used here, while the far right panel shows an example of a LBS velocity field that is poorly fit with this rotation curve form. Note that the category of galaxies that are poorly fit by a symmetric rising rotation curve (and for which we cannot obtain a reliable characteristic rotation velocity with this method) includes both objects with some evidence of disturbed rotation (as in the far right panel above) and those with no apparent rotation signature. We omit spaxels with large measured velocity errors (>15 km/s) from the plotted maps.

2/3 поддерживаются вращением